How zeolitic acid strength and composition alter the reactivity of alkenes and aromatics towards methanol

Marius Westgård Erichsen[†1], *Kristof De Wispelaere*[‡1], *Karen Hemelsoet*[‡], *Samuel L. C. Moors*[‡], *Thomas Deconinck*[‡], *Michel Waroquier*[‡], *Stian Svelle*[†], *Veronique Van Speybroeck*[‡*], *Unni Olsbye*[†*]

[†] inGAP Centre of Research Based Innovation, Department of Chemistry, University of Oslo, N-0315 Oslo, Norway

[‡] Center for Molecular Modeling (CMM), Ghent University, Technologiepark 903, B-9052 Zwijnaarde, Belgium

CORRESPONDING AUTHOR FOOTNOTE Correspondence concerning this article should be addressed to U. Olsbye at unni.olsbye@kjemi.uio.no or V. Van Speybroeck at Veronique.VanSpeybroeck@ugent.be

[1] Both authors contributed equally to this work.

Dedicated to the memory of Haldor Topsøe

Abstract:

This work encompasses a combined experimental and theoretical assessment of how zeolitic acid strength and composition affects acid catalysed methylation reactions. Overall, higher methylation rates were observed over the material with higher acid strength. Co-reactions of methanol with benzene at 250 °C over the two isostructural AFI materials H-SSZ-24 and H-SAPO-5 revealed large differences in selectivity. While the strongly acidic H-SSZ-24 mainly produced toluene and polymethylbenzenes, high yields of C_{4+} aliphatics were observed over H-SAPO-5. These results strongly suggest that alkene methylation was preferred over H-SAPO-5 even at very low conversion during methanol/benzene co-reactions. Furthermore, a comparison of benzene and propene methylation at 350-400 °C revealed a significantly faster rate of benzene than propene methylation in H-SSZ-24, whereas the rates of benzene and propene methylation were similar in H-SAPO-5. The observed difference in reactivity of the two hydrocarbons in both catalysts could be understood by careful analysis of various molecular dynamics simulations of the co-adsorbed complexes. The probability to form protonated methanol was, as expected, higher in the more acidic material. However, in H-SSZ-24 the probability for methanol protonation was higher when co-adsorbed with benzene than when co-adsorbed with propene, while the same was not observed in H-SAPO-5. Furthermore, it was found that benzene and methanol are more likely to form a reactive co-adsorbed complex in H-SSZ-24 compared to propene and methanol, while the opposite was observed for H-SAPO-5. This work shows that molecular dynamics simulations provide insights into the adsorption behaviour of guest molecules in large pore AFI materials. The obtained insights correlate with the experimentally observed reactivities.

Keywords: Methylation reactions; acid strength; ab initio molecular dynamics; co-adsorption; methanol to olefins; methanol to hydrocarbons

1. Introduction

Acid catalysis is of importance in numerous chemical reactions, not least in the petrochemical industry where zeolitic acid catalysts are used in several major processes [1]. For this reason, fundamental understanding of the effect of acid strength on reactions is a topic of major interest. The most important acid sites for catalysis over zeolitic materials are the Brønsted acidic sites formed when the negative charge resulting from a substitutional defect is balanced by a proton [2]. The strength of an isolated Brønsted acid site is most rigorously defined by the deprotonation energy of the framework. However, deprotonation energies are not easily measured for zeolites. They can be calculated by a number of theoretical methods, but accurate values are challenging to compute as different methods can give contradictory results [3]. Furthermore, deprotonation energy is an incomplete descriptor for reactivity in zeolites, as solvation effects and interactions between positively charged species and the framework contribute to the observed reactivity [4-7]. Another common measure of acid strength is the interaction of the acidic OH group with basic probe molecules, monitored by e.g. vibrational spectroscopy [8] or NMR [9]. In recent studies, it has been observed that while reaction rates globally increase when a stronger acidic catalyst is employed, the extent of the increase is not uniform for all individual reactions [10-12].

During the last decades, conversion of methanol-to-hydrocarbons (MTH) has received significant attention due to its attractiveness in processes where natural gas, coal or biomass is converted to fuels and chemicals. By tuning the catalyst and reaction conditions, a wide variety of hydrocarbons can be produced [13]. The MTH reaction is catalysed by Brønsted-acidic zeolitic catalysts. It proceeds through a complex network of reactions, referred to as the hydrocarbon pool mechanism [13-17]. The hydrocarbon pool mechanism was initially proposed by Dahl and Kolboe [18-20] and has been the subject of numerous other studies [13, 14, 16]. The hydrocarbon pool mechanism mainly consists of two interrelated reaction cycles in which polymethylbenzenes (polyMBs) and alkenes are sequentially methylated and cracked or de-alkylated to form light alkenes (see Scheme 1). These two cycles are often simply referred to as the arene and alkene cycles, respectively. The relative importance of each cycle is determined mainly by three factors: (1) catalyst topology, (2) reaction conditions and (3) acid strength. Both cycles operate simultaneously in the medium pore catalyst H-ZSM-5 [21, 22], but the arene cycle can be suppressed in the narrow channels of H-ZSM-22 [23, 24]. At similar conditions, methanol conversion over large-pore zeolites proceeds mainly via the arene cycle [25-28]. However, the reaction conditions are of great importance, as the alkene cycle can be promoted in large pore zeolites when low temperatures and high pressures are employed [29, 30]. Some of the present authors recently demonstrated that the relative importance of the arene and alkene cycle is influenced by the zeolitic acid strength [31, 32].

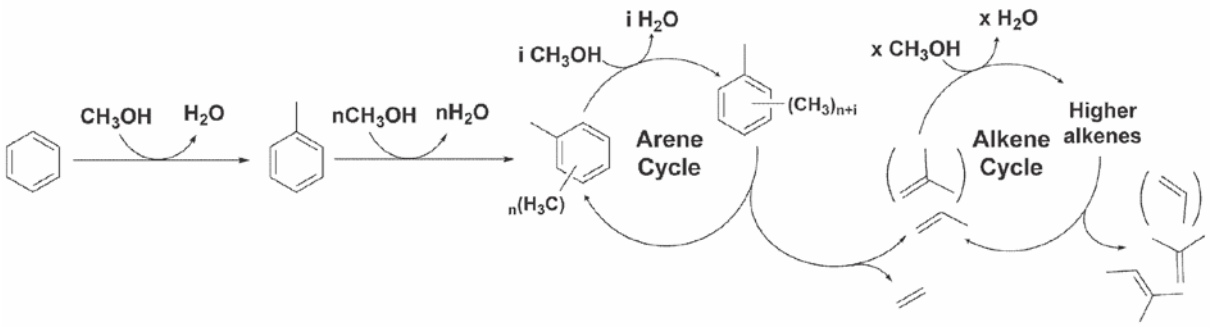

Scheme 1: Reactions expected to occur during co-reactions between benzene and methanol according to the generally accepted dual cycle mechanism [13, 31]. The reactions to the left of the scheme are expected to dominate at the chosen conditions. Benzene is first methylated to form toluene, which may be further methylated to form polymethylbenzenes. These polymethylbenzenes may de-alkylate as part of the arene cycle to yield lower alkenes. The alkenes may react further in an alkene cycle, where they are methylated to higher alkenes, and crack to form mainly branched C_4 and C_5 alkenes. It is assumed that ethene leaves the catalyst without further reaction due to its low methylation rate [75, 85, 86].

In this work, the influence of zeolitic acid strength on the methylation of arenes and alkenes was studied over the isostructural, but compositionally different, materials H-SSZ-24 and H-SAPO-5 (AFI structure). H-SSZ-24 is an aluminosilicate zeolite, while H-SAPO-5 is a silicoaluminophosphate. This difference in composition leads to a difference in Brønsted acid strength [33-35], with H-SAPO-5 containing weaker acid sites than H-SSZ-24 [32]. The AFI framework is composed of columns of twisted four- and six- rings, together forming one-dimensional twelve ring channels running parallel to the c-axis. These channels are nearly circular, and measure 7.3 Å in diameter. Previous studies on this structure demonstrated that the largest observed major product during methanol conversion is the same as during homogeneous methanol conversion, i.e. hexamethylbenzene (hexaMB) [36, 37]. Thus, the AFI topology apparently provides limited, if any, product shape selectivity. The acid strength of isolated sites is the main difference between H-SSZ-24 and H-SAPO-5 However, the difference in composition may also lead to different interaction behaviour between molecules and the framework.

The main emphasis of this work was on the reaction between methanol and benzene. Methanol/benzene co-reactions have been performed previously over the same catalysts [31, 32] but the focus of those studies was on formation of light alkenes, not on arene methylation. In the current study, experiments were performed at very low benzene conversion (< 0.3 %) in order to limit the extent of secondary reactions. Even so, significant by-product formation was observed (vide infra). A schematic overview of reactions that may occur during this co-reaction, based on the current understanding of the dual-cycle mechanism, is shown in Scheme 1. The conditions employed here were expected to strongly favour the reactions to the left in Scheme 1. In addition to monitoring product selectivity, isotopic labelling was employed to distinguish primary from secondary products.

Additional experiments were performed to directly compare rates of benzene and propene methylation over the two catalysts. These experiments were complemented with a theoretical study on the dynamical adsorption behaviour, formation of pre-reactive complexes

and reactivity of methanol and the hydrocarbons in both materials. Density Functional Theory (DFT)-based molecular dynamics and metadynamics simulations were found to illuminate the fundamental causes of the experimentally observed differences in reactivity. Recently, some of the present authors performed a molecular dynamics study on the methylation of benzene in H-ZSM-5 and discovered that prior to reaction various protonated methanol clusters can be formed. These methanol clusters seemed to have a lower reactivity towards benzene methylation as compared to single methanol molecules [38]. In this work, dynamical adsorption behaviour is for the first time linked with experimentally observed reactivities.

2. Materials and Methods

2.1. Experimental details

The synthesis of H-SSZ-24 and H-SAPO-5 has been described previously [32]. Both samples were characterized by powder X-ray diffraction, scanning electron microscopy, N_2 adsorption, n-propylamine TPD and CO-adsorption monitored by FT-Infrared spectroscopy (FTIR). More details on catalyst characterization are available in the supporting information (Section S1). FTIR-monitored adsorption of CO confirmed that H-SSZ-24 contained stronger Brønsted acidic sites than H-SAPO-5. The largest shift in O-H stretching frequency upon adsorption of CO observed in H-SSZ-24 was $\Delta\nu_{OH}$ = -317 cm^{-1}, while the shift in H-SAPO-5 was $\Delta\nu_{OH}$ = -265 cm^{-1}. Both samples were highly crystalline and exhibited similar BET surface areas (360 m^2/g and 340 m^2/g respectively). Acid site densities were determined to be 0.11 mmol/g (Si/Al ~ 150) and 0.068 mmol/g (Al+P/Si ~ 240) respectively from TPD of n-propylamine performed in a manner similar to that described by Gorte et al. [6, 39, 40]. After pre-treatment in a flow of oxygen at 550 °C, the catalyst was cooled to 150 ºC. 80 ml/min (all flows are at SATP) of N_2 bubbled through a saturator containing n-propylamine at room temperature was then fed over the catalyst for 20 minutes. Subsequently, the catalyst was left at 150 °C in a stream of 80 ml/min N_2 for 4 hours to desorb excess n-propylamine. The temperature was then ramped at 20 °C/min up to 550 °C, and the amount of propene desorbed was quantified using an on-line Pfeiffer Omnistar quadrupole mass spectrometer.

Catalytic tests were performed at atmospheric pressure in fixed bed glass reactors with catalyst powder pressed and sieved to 250-420 μm. Two otherwise identical reactors with inner diameters (i.d.) of 8 mm or 5 mm were employed. Reaction temperature was monitored by a thermocouple protected by a 3 mm wide glass sleeve inserted into the middle of the catalyst bed. ^{12}C-methanol (VWR, 99.8 %), ^{13}C-methanol (Cambridge Isotope Laboratories, 99 %), ^{12}C-benzene (Sigma-Aldrich Chromasolv, 99.9 %) and ^{12}C-propene (99.5 %, AGA) were employed as reactants. Liquid reactants were fed over the catalyst by passing a stream of helium through a flask of boiling reactant. The oversaturated helium stream was then passed upwards through a water-cooled vigreux condenser kept at constant temperature (typically 30°C for methanol and 35°C for benzene) by a circulating thermostat water bath. A range of partial pressures and space velocities could be obtained by adjusting the flow of either reactant or a third gas line with pure helium.

Co-reactions between 60 mbar of ^{12}C benzene and a variable partial pressure of ^{12}C or ^{13}C methanol at 250 °C and 350 °C were performed over both catalysts at conditions chosen to obtain low conversion of either reactant. For H-SAPO-5, 40 mg of catalyst in an 8 mm i.d. reactor and a constant total flow of 54.5 ml/min was used, leading to WHSV = 22 $g_{feed}\, g_{catalyst}^{-1}\, h^{-1}$ at partial pressures (P) of 60 mbar for each reactant. For H-SSZ-24, 10 mg catalyst in a 5 mm i.d. reactor was used with a constant total flow of 109 ml/min for a WHSV = 174 $g_{feed}\, g_{catalyst}^{-1}\, h^{-1}$ at P = 60 mbar for each reactant. Two series of experiments (one at each temperature) were performed for each catalyst, where the catalyst was first activated in a flow of oxygen at 550 °C for 1 hour before cooling to reaction temperature and the introduction of reactants. Analyses were performed after 10 minutes time on stream, assuming steady state activity. Between each measurement, the catalyst was regenerated in oxygen at 550 °C for 1 hour. A slight decrease in catalyst activity was observed between each measurement. The effects of deactivation on our conclusions were minimized by varying partial pressures in a random order and by periodically returning to a set of standard conditions. By comparing the catalyst activity for each measurement at these conditions, a function describing the activity loss in intermediate measurements was derived: $y = ax^b$, where y is acid site density and x is the measurement number. This procedure allowed us to report data corrected for deactivation. An example is provided in the supporting information, Section S2.5.

The rates of benzene and propene methylation were compared at 350 °C and 400 °C. In these experiments, 2.5 mg H-SSZ-24 or 10 mg H-SAPO-5 diluted in 50 mg of quartz (250-420µm) was used in a 5 mm reactor. 60 mbar of methanol was co-reacted with 60 mbar of either benzene or propene, giving WHSV = 762 h^{-1} or 512 h^{-1} respectively over H-SSZ-24 (total flow was 120 ml/min) or 95 h^{-1} or 68 h^{-1} respectively over H-SAPO-5 (total flow was 60 ml/min). The effluent was analysed after 10 minutes of reaction. For the comparison, benzene and propene methylation experiments were performed alternately. Between each measurement, the catalyst was regenerated for 90 minutes in O_2 at 550 °C.

Both the situation where 2.5 mg catalyst was diluted in 50 mg quartz, and when 10 mg catalyst was used alone were checked for bypass by confirming that full conversion of 2-propanol to propene at 200 °C could be achieved in both cases.

Effluent from the reactor was analysed quantitatively by online GC/MS analysis (Agilent 7890 with flame ionisation detector and 5975C MS detector) using two Restek Rtx-DHA-150 columns (150 m, 0.25 mm i.d., stationary phase thickness 1 µm) attached to the same inlet but different detectors. H_2 (purity 6.0, AGA) was used as carrier gas.

2.2. Computational details

Ab initio calculations in a fully periodic AFI catalyst model were carried out with the CP2K simulation package [41, 42], using a DFT level of theory with a combination of Gaussian and plane wave basis sets (GPW) [43, 44]. The revPBE functional was chosen for its improved catalytic energies compared with the commonly used PBE functional for solid-

state calculations [45]. The DZVP-GTH basis set and pseudopotentials were used [46], and the Grimme DFT-D3 approach was applied to account for the attractive van der Waals interactions [47]. The AFI 1x1x2 super cell consists of 145 atoms (Figure S4.1) and contains one Brønsted acid site, which corresponds to Si/Al and (Al+P)/Si ratios of 47 for SSZ-24 and SAPO-5, respectively. Note that this ratio corresponds to a higher acid site density compared to the samples employed for experiments (150 and 240 respectively). However, the acid site density was still low enough to assume that neighbouring acid sites do not affect each other during reactions. The shortest distance between two acid sites in the same channel was approximately 17 Å and between two acid sites in adjacent channels 14 Å, indicating that we indeed simulated isolated acid sites. It has previously been found that the rate (per acid site) of propene oligomerisation over H-MFI was affected by the Si/Al ratio for values between 12 and 40, but that a further increase from Si/Al 40 to 140 did not affect the rate [48]. Moreover, mimicking a lower acid site density would require the use of larger super cells, which would increase the computational demands extensively. That the applied models exhibit the expected different acid strengths of the isostructural materials was demonstrated by the observed O-H bond elongation upon methanol adsorption during a high temperature MD simulation (see Supporting Information, Section S5). The catalyst's hydroxyl bond length varied in a wider distance range in H-SSZ-24 than in H-SAPO-5. Accordingly, the probability to sample protonated methanol was 9% in H-SSZ-24, whereas it was only 1% in H-SAPO-5, which is also directly related to the acid strength. These probabilities correspond to free energy differences for methanol protonation of 12 and 24 kJ/mol respectively.

Ab initio molecular dynamics (MD) simulations were performed to assess the adsorption behaviour of the guest molecules at realistic reaction temperatures (350 ºC). After an equilibration run of 5 ps, a production run of 50 ps was performed in the NPT ensemble at 1 bar and 350 ºC in which the zeolitic framework is fully flexible. The temperature was controlled via a chain of 5 Nosé-Hoover thermostats. The time-averaged cell parameters were obtained from the NPT MD simulations with the appropriate guest molecules adsorbed in the framework and are summarized in the Supporting Information (Section S4). An integration time step of 0.5 fs was applied. A selection of snapshots from the MD simulations was used as input for static geometry optimizations on some relevant adsorption complexes. To calculate the probability that a pre-reactive complex for methylation is formed during an MD simulation of methanol and a co-adsorbed hydrocarbon, the difference between the shortest methanol oxygen – hydrocarbon carbon distance and the shortest methanol carbon - hydrocarbon carbon distance was traced (Supporting information, Figure S4.2). A sampled state where this difference was higher than 0.5 Å was considered to resemble a pre-reactive complex, as the methyl group then pointed towards the benzene or propene molecule. The cut-off value of 0.5 Å was chosen arbitrarily, but performing the analysis with other positive cut-off values yielded the same trends. From the MD runs, the probability to protonate methanol was computed based on a distance criterion; methanol was considered to be protonated if the distance between the Brønsted acid proton and the methanol oxygen was below 1.2 Å. Free energy differences between protonated and neutral methanol were computed from the relative populations of both stable states during an entire MD run, using the following equation [49]:

$$\Delta G_{A,B} = -RT\ ln\frac{P(A)}{P(B)} \qquad (1)$$

where P(A) and P(B) are the relative populations or probabilities for stable states A and B.

Geometry optimizations were performed based on MD snapshots to calculate (co-) adsorption energies using the purely electronic energy values, including dispersion corrections. Hereby, it was checked whether conformations found as stable potential energy minima in one material were also minima in the other material. Additionally, transition states were localized using the dimer method implemented in CP2K. A normal mode analysis was performed to confirm that the optimized transition states were true first order saddle points. To determine the pre-reactive complex and products, a quasi-irc approach was applied. Theoretical procedures to accurately determine barriers for alkene methylations are currently available [50-53]; however, procedures as applied in previous studies on H-ZSM-5 are not straightforwardly applicable to the AFI topology. First of all, a finite cluster is insufficient to describe the one dimensional large pore channels appropriately and thus periodic zeolite models are preferred. Secondly, the large pores enable guest molecules to adopt many configurations, for which a static approach based on one transition state is probably too limited (*vide infra*). Therefore, a further assessment of reactivity was performed with metadynamics simulations, which is a technique to enhance rare event sampling developed by Laio and Parrinello [54, 55]. During these simulations, coordination numbers (CN in Eq. 2) were selected as collective variables.

$$CN = \sum_{i,j} \frac{1-\left(r_{ij}/r_0\right)^{nn}}{1-\left(r_{ij}/r_0\right)^{nd}} \qquad (2)$$

where the sum runs over two sets of atoms i and j, r_{ij} is the distance between atoms i and j and r_0 is a reference distance. For all coordination numbers used in this study, a reference distance r_0 of 2.0 Å was chosen, as this value lies in the range of typical transition state distances of the bonds that have to be broken and formed during a methylation reaction. The parameters nn and nd are set to 6 and 12, respectively. With these coordination numbers as switch function defining the order parameters, unbonded states are mapped on values close to zero, transition states on values around 0.5 and fully bonded states on values around 1. Quadratic walls were used to restrict the exploration of the Free Energy Surface (FES) to a particular area of interest (Supporting Information S4). The reacting methanol molecule is kept close to the acid site and the product region is not entirely sampled to prevent the formation of more stable toluenium cations and as such enhance barrier recrossings. Hills with a height of 5.8 kJ/mol and a width of 0.02 were spawned every 50 time steps (25 fs). The total simulation time was 47 ps, which was enough to sample all transitions at least once. The simulation was performed in the CP2K software in the NVT ensemble at 350 °C. The temperature during the simulations is controlled by a chain of 5 Nosé-Hoover thermostats. In this study, we use the metadynamics technique for sampling. More extensive simulations would be required to obtain accurate free energy profiles to perform a complete kinetic analysis. However, this falls beyond the scope of this article. Note that there are only a few studies applying MD based techniques to study zeolite-catalysed reactions [56-61]. A comprehensive review on various

theoretical procedures applied to study zeolite-catalysed reactions can be found in reference [62].

3. Results and discussion

3.1. Co-reactions between benzene and methanol

Net rates of product formation during co-reactions between benzene and methanol at 250 °C are shown in Figure 1. Globally, the stronger acid H-SSZ-24 yielded ~4 times higher benzene conversion rates (per acid site) than the weaker acid catalyst H-SAPO-5. Although the experiments were performed at differential conversions (>0.3 % benzene conversion) in an attempt to suppress secondary reactions, by-product formation was still observed over both catalysts. The by-products observed were mainly polymethylbenzenes, diphenylmethane and aliphatic products. Detailed product selectivities from co-reaction of benzene and methanol in a 1:1 molar ratio are included in the supporting information (Section S2.1). As the isotopic distributions of the aromatic products were found to be consistent with (successive) methylation of ^{12}C benzene by ^{13}C methanol (Section S2.2), this means that the conversion of methanol was higher than the conversion of benzene.

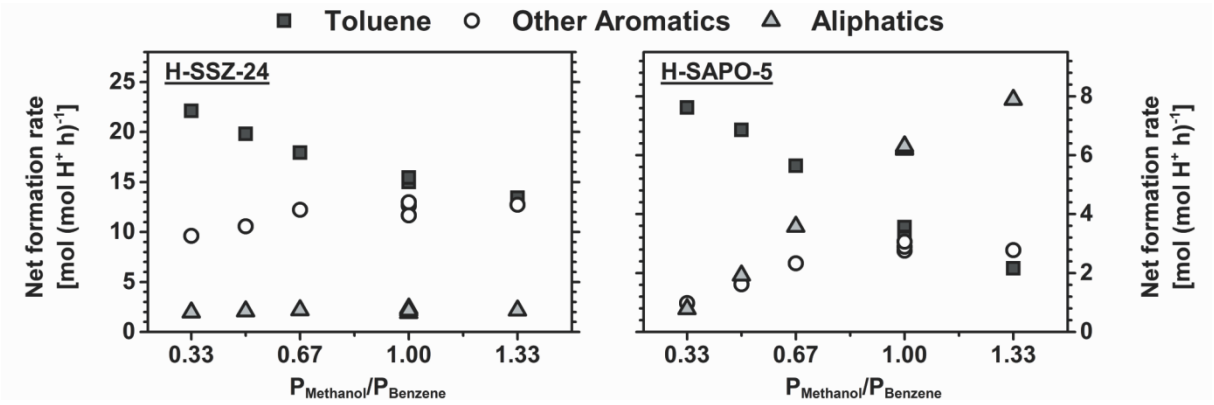

Figure 1: Net rates of formation of the main product groups during co-reactions of benzene and methanol as a function of the methanol to benzene molar feed ratio at 250 °C over H-SSZ-24 (left) and H-SAPO-5 (right). $P_{Benzene}$ = 60 mbar. Benzene feed rate = 13×10^3 mol (mol H^+)$^{-1}$ h^{-1} over H-SSZ-24 and 2.9×10^3 mol (mol H^+)$^{-1}$ h^{-1} over H-SAPO-5. Total WHSV = 140-191 h^{-1} (H-SSZ-24) or 17.5-24 h^{-1} (H-SAPO-5). The data have been corrected for deactivation.

As observed from Figure 1, the primary product toluene dominated in both catalysts at a 1:3 ratio of methanol to benzene (P_{MeOH} = 20 mbar). However, successive over-methylation products and diphenylmethane were observed, especially in H-SSZ-24. At higher methanol partial pressures, the differences between the two catalysts increased. Over H-SSZ-24 (Figure 1, left) the net formation rate of other aromatics increased slightly with increasing $P_{MeOH,}$ at the expense of the net toluene formation rate. A high rate of successive methylation to form polyMBs is consistent with an increasing methylation rate per methyl group present on the aromatic ring [12, 63-66]. Overall, the benzene conversion rate decreased slightly with

increasing methanol pressure (from 0.21 to 0.18 %), while the rate of methanol conversion remained constant. The curve for the net rate of aliphatics formation closely resembled the other aromatics, maintaining a molar ratio of other aromatics to aliphatics between 5 and 6.

Figure 1 (right) shows that over H-SAPO-5, similarly to what was observed over H-SSZ-24, an increase in methanol partial pressure led to a decrease in the net rate of toluene formation due to over-methylation to other aromatics. Unlike what was observed over H-SSZ-24, the rate of aliphatic formation increased rapidly with increasing methanol pressure over H-SAPO-5. At a 1:1 molar feed ratio of benzene and methanol, aliphatic products accounted for about 50 % of the total molar amount of products formed. Furthermore, the formation rates of aliphatics and other aromatics were not correlated, in contrast to what was found over H-SSZ-24. The increased net rate of aliphatics formation was accompanied by a significant decrease in benzene conversion at higher P_{MeOH}. While 0.27 % of the benzene feed was converted over H-SAPO-5 at the lowest molar feed ratio (methanol/benzene = 0.33), benzene conversion was only 0.16 % at the highest molar feed ratio (1.33).

The remarkably different behaviour of aliphatics formation rates in the two catalysts warrants a closer look at the detailed aliphatics distributions. Figure 2 displays the distribution of aliphatic products produced over the two catalysts, grouped by their carbon number, as a function of the molar feed ratio. As seen from Figure 2, the type of aliphatics formed differs significantly for the two catalysts. Over H-SSZ-24, mainly ethene and propene was formed, with smaller amounts of C_4 and C_{5+}. The distribution of aliphatics in Figure 2 is similar, over the entire range of methanol/benzene feed ratios, to that previously observed from the arene cycle in the same catalyst [32]. Together with the relatively constant ratio of aliphatics to polyMBs (Figure 1, left), this strongly suggests that aliphatic products were formed mainly by polyMB de-alkylation (i.e. the arene cycle - see Scheme 1).

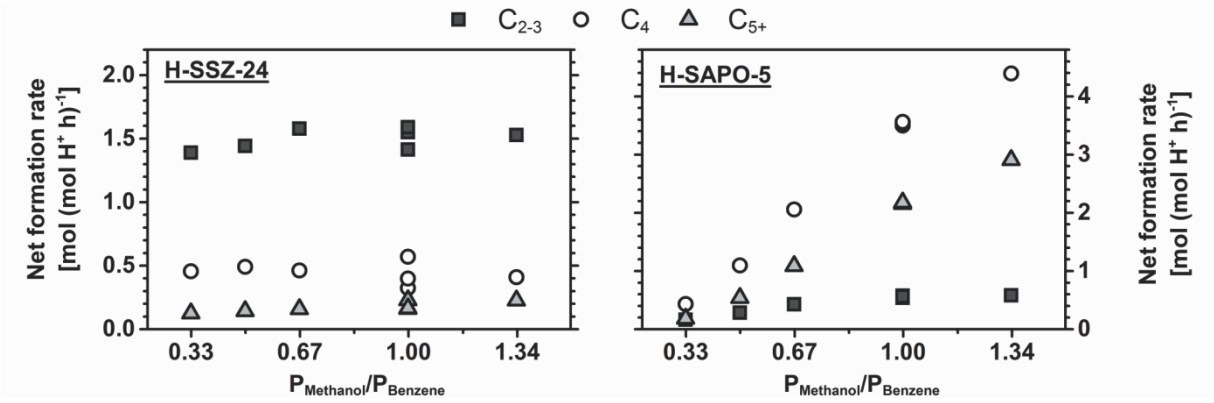

Figure 2: Net rates of formation for aliphatic products during co-reactions of benzene and methanol as a function of the methanol to benzene molar feed ratio at 250 °C over H-SSZ-24 (left) and H-SAPO-5 (right). $P_{Benzene}$ = 60 mbar. Benzene feed rate = 13×10^3 mol (mol H^+)$^{-1}$ h^{-1} over H-SSZ-24 and 2.9×10^3 mol (mol H^+)$^{-1}$ h^{-1} over H-SAPO-5. Total WHSV = 140-191 h^{-1} (H-SSZ-24) or 17.5-24 h^{-1} (H-SAPO-5). The data have been corrected for deactivation.

In contrast, Figure 2 reveals that H-SAPO-5 produces much more C_4 and C_{5+} than H-SSZ-24 and that these become more abundant relative to C_{2-3} at higher methanol/benzene feed

ratios. Previous studies have shown that C_4 and C_{5+} aliphatics were predominantly formed via the alkene cycle in H-SAPO-5, while ethene and some propene was formed from polyMB de-alkylation [31, 32]. The high rates of higher aliphatics formation observed over H-SAPO-5 in this work thus strongly suggests that the main pathway to aliphatics formation over H-SAPO-5 was via alkene methylation and cracking (i.e. the alkene cycle - see Scheme 1).

It is difficult to extract the exact ratio of products originating from the arene and alkene cycles since many of the same products are produced by both cycles. However, as C_{2-3} aliphatics mainly originate from the arene cycle while C_{5+} aliphatics are predominantly formed in the alkene cycle (see Scheme 1), a low C_{2-3}/C_{5+} provides an indication of the relative importance of each cycle. A high ratio implies that the arene cycle dominates, while a low ratio implies that the alkene cycle dominates. Over H-SSZ-24, this ratio was 8 at a 1:1 molar feed ratio, while it was 0.25 over H-SAPO-5 at the same feed ratio. This implies a much higher influence of the alkene cycle over H-SAPO-5 than over H-SSZ-24.

A high influence of the alkene cycle over H-SAPO-5 under these conditions indicate that alkene methylation is strongly favoured relative to benzene methylation over H-SAPO-5, as the concentration of benzene in the effluent was 2-3 orders of magnitude higher than the concentration of aliphatics. This result furthermore contrasts the results obtained for the more strongly acidic H-SSZ-24 where (successive) methylation of benzene dominates and the small amount of aliphatics formed originate from polyMB de-alkylation.

While hydrocarbon formation was the main focus of this work, dimethyl ether (DME) was also formed over both catalysts (Figure S2.3). It was observed that while no more than 2 % of the methanol was converted to DME over H-SSZ-24, the yields of DME over H-SAPO-5 were between 16 and 62 %. A plausible explanation for this extremely high yield of DME over H-SAPO-5 is that H-SAPO-5 contains additional sites capable of catalysing methanol dehydration to form DME. Previous works have shown activity for DME formation over pure aluminophosphate catalysts [67, 68], possibly due to the presence of weakly acidic P-OH groups. Such sites are commonly observed in H-SAPO-5 materials (see S1 and [69-71]) and may be acidic enough to dehydrate methanol, while still being inactive for C-C bond formation. However, DME and methanol are usually assumed to behave similarly as methylating agents, although with slightly higher methylation activity for DME [72-74]. Therefore, DME was treated as a reactant rather than a product in this work.

Similar co-reaction experiments were performed at 350 °C, and the results are included in the supporting information (Section S2.4). At this temperature, successive methylations, leading predominantly to penta- and hexaMB, and formation of aliphatics by polyMB de-alkylation was more prominent over both catalysts than at 250 °C. Furthermore, isotopic distributions revealed a high degree of carbon scrambling (Figure S2.6 and S2.7), which complicated the analysis of the reaction. The selectivity difference between the two samples was less dramatic at 350 °C than at 250 °C, but differences were still observed related to aliphatics formation. Similarly to at 250 °C the net rate of aliphatics formation in H-SAPO-5 increased faster with increasing P_{MeOH} than in H-SSZ-24, and the C_{2-3}/C_{5+} ratio was also significantly lower over H-SAPO-5 than over H-SSZ-24 (3.5 versus 12, respectively).

Both of these observations indicate that methylation of aliphatics was more prominent in H-SAPO-5 than in H-SSZ-24 also at 350 °C. Another complication arose from the high conversion of methanol to DME over H-SAPO-5 at this temperature (>70 % compared to 3 – 4 % in H-SSZ-24). The effect of DME versus methanol as methylating agent was investigated over H-SSZ-24. It was found that the main difference between DME and methanol was a faster overall reaction rate when DME was used (Figure S2.6). To summarize, the trends observed at 250 °C were reproduced at 350 °C, although the added complexity of high conversion and more side-reactions made interpretation less straightforward.

3.2. Experimental comparison of benzene and propene methylation

The results obtained in Section 3.1 strongly indicate that in H-SAPO-5 methylation of alkenes was strongly favoured relative to methylation of aromatics, while a similar preference was not observed over the stronger acid H-SSZ-24. Verification of this hypothesis was sought by direct comparison between the methylation rates of propene and benzene over H-SAPO-5 and H-SSZ-24. To obtain a more fundamental understanding of the reactivity of benzene and propene in both materials, a molecular dynamics study was performed to link the dynamical behaviour of co-adsorbed complexes with the observed reactivity towards methylation (*vide infra*).

In principle, the experimental rate comparison was straightforward: methanol was co-fed with either benzene or propene at a predetermined set of conditions (T = 350 - 400 °C, $P_{MeOH} = P_{co\text{-}reactant}$ = 60 mbar) over the same catalyst batch. In practice, however, each co-feed experiment was complicated by a set of parallel and sequential reactions characteristic of the hydrocarbon used. Using benzene, the selectivity to toluene (the primary methylation product) decreased with increasing methanol/benzene feed rate (see Section 3.1). On the other hand, during co-reactions of methanol and propene low methanol/propene feed rates resulted in high rates of propene dimerization. Furthermore, the rate of propene dimerization over H-SSZ-24 was observed to decrease with increasing temperature, in line with what has previously been reported by Svelle et al. [75] over H-ZSM-5. An acceptable compromise of conditions was found at 400 °C, with significantly higher feed rates than employed in Section 3.1 and a methanol : co-reactant molar ratio of 1:1. The higher feed rates resulted in less than 1.2 % conversion of the hydrocarbon.

At these conditions toluene selectivities of approximately 50 mol % and 35 mol % were obtained over H-SSZ-24 and H-SAPO-5 respectively during co-reactions of methanol and benzene. For methanol/propene co-reactions, the selectivity to n-butenes (the primary methylation product) was 29 mol% and 43 mol% in H-SSZ-24 and H-SAPO-5 respectively. The dominant by-products during methanol/benzene co-reactions were polyMBs. An overview of the experiments, including conversion and selectivities is given in Section S3.1. During methanol/propene co-reactions the by-products were more diverse, but the most prominent were branched C_4 aliphatics (i-butene and i-butane) and C_6 alkenes. The isotopic distributions suggested that C_6 alkenes were mainly formed from dimerization of propene,

while branched C_4, aromatic and other aliphatic compounds (C_{2-5}) resulted from a combination of C_4 methylation and cracking (Section S3.2).

Net formation rates for the primary methylation product from each co-feed experiment are shown in Figure 3. MS analysis confirmed that the primary methylation products in all experiments contained one ^{13}C atom originating from methanol (Section S3.2). While the selectivity to these primary products was too low to represent a comparison of the absolute methylation rates, they nevertheless provide a qualitative comparison. The net rate of toluene formation from benzene methylation was found to be three times higher than that of n-butene formation from propene methylation over H-SSZ-24 at 400 °C. This difference was not observed over H-SAPO-5. Instead, the net rate of n-butene formation was only slightly lower than the net rate of toluene formation over H-SAPO-5. Considering instead the total conversion of all reactants, a similar trend was found (Figure S3.1): the total conversion of both reactants was nearly twice as high during benzene co-reaction as during propene co-reaction over H-SSZ-24, while similar conversion was observed for the two reactions over H-SAPO-5. This means that the observed difference in methylation activity displayed in Figure 3 cannot be ascribed simply to a difference in product selectivity. Together, the results from direct comparison of propene and benzene methylation correspond well with the observations from Section 3.1, namely that the ratio between methylation of aromatics and methylation of aliphatics was higher in the strongly acidic catalyst H-SSZ-24 than in the weaker acid H-SAPO-5.

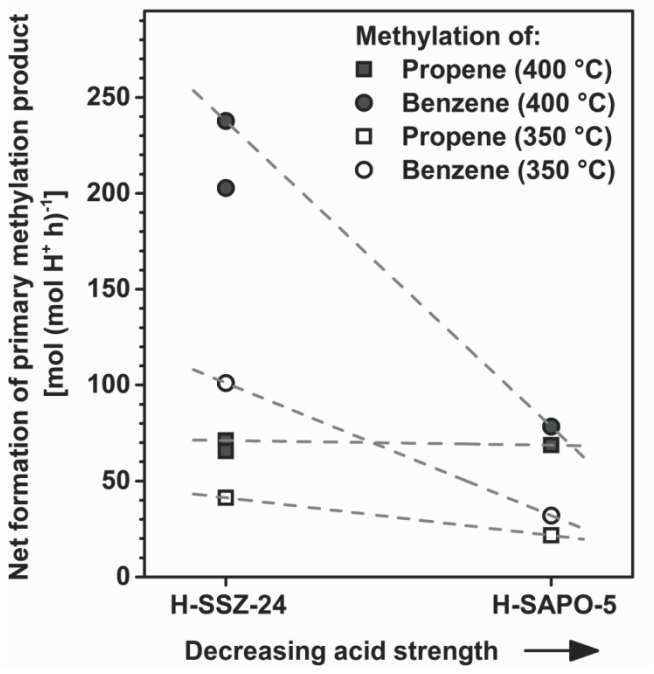

Figure 3: Rates of formation for n-butenes (squares) and toluene (circles) during co-reactions of methanol and propene or benzene, respectively, at 400 °C and 350 °C over H-SSZ-24 and H-SAPO-5. All reactant partial pressures were 60 mbar. The data for H-SAPO-5 has been corrected for deactivation, but raw data is reported for H-SSZ-24 as no clear deactivation trend was observed. Thus, there are 2 different data points each for propene and benzene methylation over H-SSZ-24 at 400 °C. Feed rates of propene/benzene/methanol = 6.9×10^3 mmol g_{cat}^{-1} h^{-1} (H-SSZ-24) and 0.87×10^3 mmol g_{cat}^{-1} h^{-1} (H-SAPO-5).

Similar experiments were performed at 350 °C in order to more directly compare with the results of Sections 3.1 and 3.3. The results are displayed together with those at 400 °C in Figure 3. While toluene selectivities of 45 mol% were achieved in both materials during methanol/benzene co-reactions, much lower n-butene selectivities were achieved during methanol/propene co-reactions than at 400 °C (22 mol % over H-SSZ-24 and 33 mol% over H-SAPO-5). The main reason for the low selectivity to n-butenes at 350 °C was an increased selectivity to propene dimerization. This was especially prominent for H-SSZ-24, where the rate of propene dimerization increased when temperature was decreased from 400 °C to 350 °C. An increased selectivity to C_6 alkenes was observed also in H-SAPO-5, but their net rate of formation decreased with decreasing temperature. The poor selectivity for propene methylation complicates the comparison of the methylation rates, but the qualitative indications from the experiments at 350 °C fall in line with the experiments at 400 °C and the results of section 3.1. Figure 3 clearly shows similar net rates of benzene and propene methylation over H-SAPO-5, but a significantly higher net rate of benzene methylation compared to propene methylation over H-SSZ-24 at 350 °C.

In summary, the results obtained in this study suggest that benzene methylation is affected more by a change in acid strength than propene methylation. It has previously been proposed that reactions involving diffusely charged transition states are more sensitive to changes in acid strength than those containing more localised charges [10, 11]. It is plausible that the positive charge in the transition state of arene methylation is more diffusely distributed than during alkene methylation. In this case, a higher dependency on acid strength for the rate of benzene methylation than propene methylation would be expected. The data obtained in this work does not warrant a full kinetic analysis due to the many complicating side-reactions, but the qualitative indications remain the same throughout a fairly wide range of conditions.

3.3. Theoretical comparison of benzene and propene methylation

3.3.1. Adsorption behaviour from molecular dynamics simulations

To get a thorough understanding of the experimentally observed difference in reactivity of benzene and propene towards methylation in both AFI materials, MD simulations of co-adsorbed methanol-benzene and methanol-propene complexes were performed. Two indices were defined: the probability of forming co-adsorbed complexes exhibiting a proper orientation for methylation and the probability of forming a protonated methanol molecule. For this analysis, MD techniques were required to sample all possible orientations of the reactants appropriately. During the MD simulations at 350 ºC, the zeolitic framework simulation cell was loaded with 1 methanol and 1 benzene or propene molecule, and a 50 ps simulation was run. It was observed that methanol, rather than benzene or propene, covered the acid site throughout nearly the entire simulation in both materials. This was due to a relatively strong hydrogen bond between methanol and the Brønsted acid site. During the first couple of picoseconds of each simulation, methanol repelled the hydrocarbon from the acid

site, as depicted for methanol and benzene in H-SAPO-5 in Figure 4. Methanol was considered to occupy the acid site if the distance between the methanol oxygen and the framework oxygens surrounding the substitutional defect was shorter than 3.5 Å (Supporting Information, section S6). That methanol mainly occupied the acid site implies that hydrocarbons suitable for methylation will be co-adsorbed and interact with the framework and methanol, but not directly with the acid site. This could also be concluded by tracing the shortest hydrocarbon – acid site distance and the orientation of the co-adsorbed hydrocarbons in the AFI channel (Supporting Information, S6).

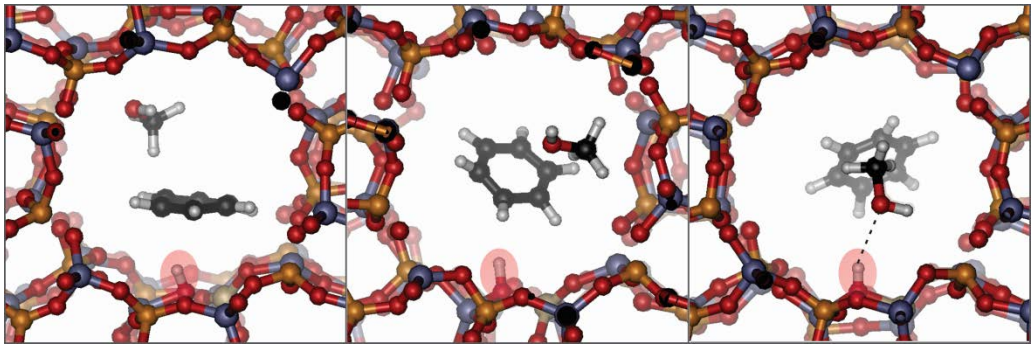

Figure 4: Left: Initial structure with benzene occupying the acid site and MeOH co-adsorbed in H-SAPO-5. Middle: during the first 1-2 ps of the MD simulation at 350 ºC methanol replaces benzene on the acid site. Right: methanol remains adsorbed on the acid site throughout the rest of the simulation. The acid site is highlighted.

Subsequently, geometry optimizations based on some relevant snapshots of the MD simulations were performed to get a detailed insight into the various stable co-adsorbed complexes that can be formed. Except for the co-adsorption of benzene in H-SSZ-24, two stable co-adsorption complexes of methanol and benzene or propene could be located on the potential energy surface at 0 K. One of these geometries strongly resembles a pre-reactive complex for the methylation reaction (Figure 5 (a) and (c) for benzene and propene co-adsorption respectively). A selection of the most important optimized co-adsorption complexes is displayed in Figure 5; a complete overview of all structures in both catalysts is given in Figure S7.1 and Figure S7.2. The corresponding adsorption energies for the selected snapshots are summarized in Table S7.1. The reported adsorption energies are purely electronic values and may give some insight into the interaction strength between guest molecules and the host material. A complete analysis of enthalpic and entropic contributions to fully understand the adsorption thermodynamics is beyond the scope of this article.

As expected, methanol adsorption was stronger in the more acidic H-SSZ-24 (-98.4 kJ/mol versus -83.2 kJ/mol in H-SAPO-5). Co-adsorption of benzene or propene was energetically slightly more favourable in H-SAPO-5 (-84.6 or -88.9 kJ/mol for benzene, -67.5 or -59.5 kJ/mol for propene) than in H-SSZ-24 (-80.5 kJ/mol for benzene, -51.6 or -53.9 kJ/mol for propene), pointing to stronger interactions between guest molecules and the more polar silicoaluminophosphate. For H-SAPO-5, two energetically equivalent[1] methanol/benzene co-adsorption complexes were found: with the methanol methyl group

[1] For the DFT calculation performed here, energy differences up to 5 kJ/mol are considered as insignificant.

either pointing towards (Figure 5a) or away from (Figure 5b) benzene. For H-SSZ-24 the latter could not be located as a potential energy minimum. Two similar minima could be located on the potential energy surface in both structures (Figure 5c and d) for propene co-adsorption. In H-SSZ-24 the two stable states were energetically equivalent, whereas in H-SAPO-5 there was a slight preference for co-adsorption with a direct methanol proton – π-electron interaction (shown in Figure 5d). The multiple localized potential energy minima indicate the complexity of the potential energy surface (PES) of the co-adsorbed molecules in this large pore zeolite material, hence molecular dynamics is a useful tool to sample larger portions of this PES.

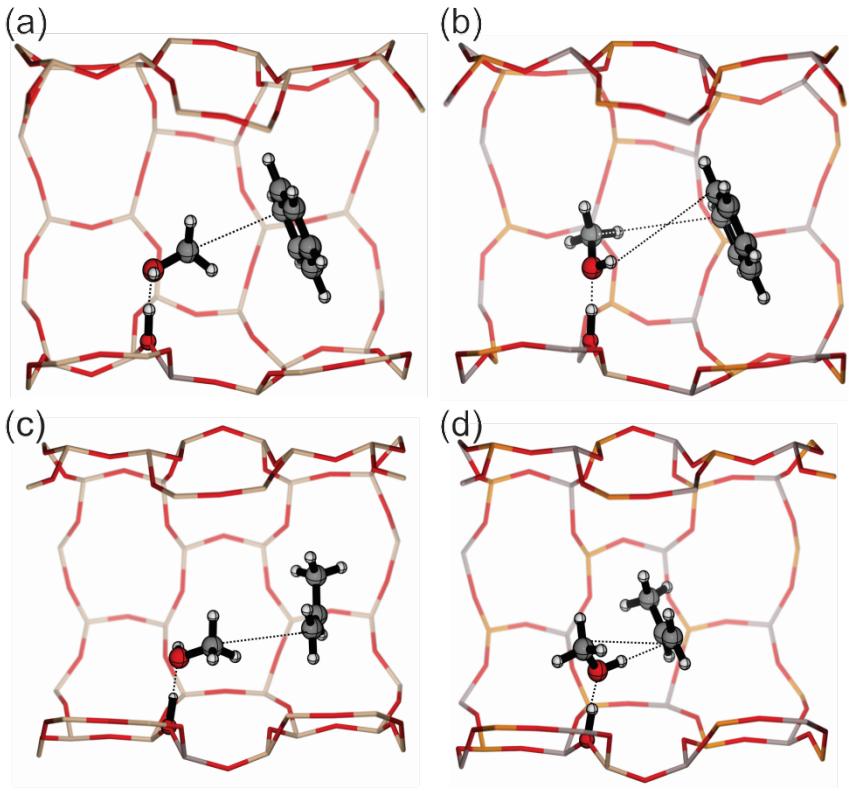

Figure 5: Optimized co-adsorbed complexes of methanol and benzene (a,b) and methanol and propene (c,d) in H-SSZ-24 and H-SAPO-5. Complexes a, c, and d apply for both H-SSZ-24 and H-SAPO-5.

To clearly demonstrate the differences between the two materials, the probabilities of finding protonated methanol complexes and pre-reactive complexes for methylation during the MD runs were calculated, as both quantities can be related to the methylation reactivity of the co-adsorbed compounds (*vide infra*). Experimental and theoretical studies earlier reported on the importance and role of protonated methanol during zeolite-catalysed methanol conversions [76-78]. The average shortest carbon-carbon interaction distances between methanol and benzene during the MD simulations at 350 ºC were 5.41 Å and 5.61 Å in H-SSZ-24 and H-SAPO-5 respectively. A shorter carbon-carbon atom interaction distance suggests a slightly higher methylation reactivity, as the distance the methyl group will have to bridge to form a transition state is smaller. To confirm the latter, we calculated transition states and the corresponding pre-reactive and product complexes for benzene methylation

(Figure S8.1). The pre-reactive complex indeed resembled the states identified during the MD run with shorter C_{MeOH} - $C_{benzene}$ distance. The electronic energy barriers found for benzene methylation were 123 and 134 kJ/mol in H-SSZ-24 and H-SAPO-5 respectively. The lower activation barrier for the reaction in H-SSZ-24 is in line with its higher acidity. A detailed kinetic analysis based on optimized transition states is beyond the scope of this study, but has been reported earlier for benzene methylation in H-ZSM-5 and H-beta [52]. Moreover, a kinetic analysis based on one single transition state only gives a limited amount of information as the potential energy surface is too complex to be fully captured with a static approach (*vide infra*). To distinguish structures resembling the pre-reactive complex from other sampled states in the MD simulations at 350 ºC, the difference between the shortest methanol oxygen – benzene carbon distance and the shortest methanol carbon - benzene carbon distance was measured (Figure S4.2). A sampled state where this difference was higher than 0.5 Å was considered to resemble a pre-reactive complex, as the methyl group pointed towards the benzene ring. The probability to sample a pre-reactive complex was 35 % in H-SSZ-24 and 17 % in H-SAPO-5 (vertical axis in Figure 6). Furthermore, the distances between the methanol oxygen and the Brønsted acid proton during the MD runs of methanol and benzene indicated that methanol was protonated 9 % of the time in H-SSZ-24, but only 2 % of the time in H-SAPO-5 (horizontal axis in Figure 6). From the relative population of the protonated and deprotonated state of methanol (Eq. 1), free energy differences of 12 kJ/mol and 21 kJ/mol are obtained for protonation of methanol in the co-adsorbed complexes in H-SSZ-24 and H-SAPO-5 respectively. This observation is of course straightforwardly correlated with the higher acid strength of H-SSZ-24 [79] (see Supporting Information S5). It should be mentioned that the quantities on both axes are not expected to be fully uncorrelated. Due to the charge transfer that occurs during methanol protonation, the interactions between methanol and benzene or propene will be slightly altered.

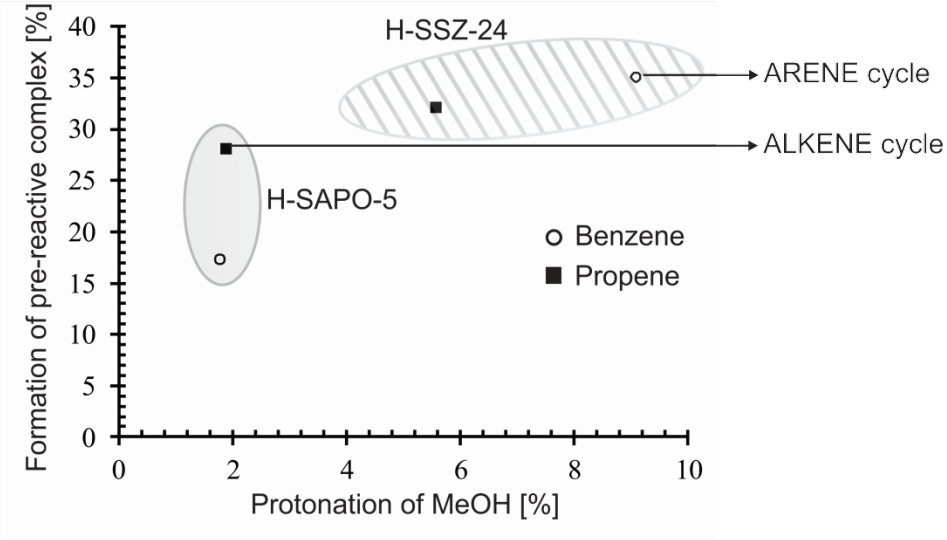

Figure 6: Degree of protonation of methanol versus the probability for the formation of a pre-reactive complex at 350 ºC for benzene and propene in H-SSZ-24 (shaded area) and H-SAPO-5 (filled area).

For co-adsorbed propene and methanol, the average shortest methanol carbon – propene carbon distances from the MD simulations were 5.83 Å in H-SSZ-24 and 5.54 Å in H-SAPO-5. In H-SSZ-24, this distance was significantly larger than for the corresponding co-adsorption complex for methanol and benzene (5.41 Å). In H-SAPO-5, the opposite was observed: the shortest methyl carbon – propene bond was slightly shorter than what was observed for benzene co-adsorption (5.61 Å). An overview of the time-averaged shortest distances is given in Figure S9.1. Furthermore, the optimized structure with the shortest methanol carbon – propene carbon distance (Figure 5c) looks like a pre-reactive complex for the methylation reaction, indicating that a geometrical analysis of the MD simulation can reveal useful information on the behaviour of the co-adsorbed system. For propene methylation, no true first-order saddle point could be located in either of the AFI materials. Detailed kinetic studies on propene methylation in various zeolites were reported elsewhere [51, 53]. To compute the probability for sampling a pre-reactive complex during an MD run, the same procedure as described above for benzene co-adsorption was applied. The probabilities of sampling geometries in which the methanol methyl group points towards propene were 32 % and 28 % for H-SSZ-24 and H-SAPO-5 respectively (vertical axis in Figure 6). An analysis of the degree of methanol protonation in presence of propene further indicated that methanol was protonated during 6 % of the simulation time in H-SSZ-24, and 2 % of the simulation time in H-SAPO-5 (horizontal axis in Figure 6). The corresponding free energy differences were 15 and 20 kJ/mol for protonation of methanol with co-adsorbed propene in H-SSZ-24 and H-SAPO-5 respectively.

While the probability to form a pre-reactive complex with benzene was twice as high in H-SSZ-24 as in H-SAPO-5, the formation probabilities of a pre-reactive complex with propene in the two catalysts were very similar. The ease of methanol protonation and the probability to form a favourable pre-reactive complex for methylation, as shown in Figure 6, can be related to the reactivity of benzene and propene towards methylation in both AFI materials (see Section 3.3.2). From the experiments reported in Section 3.1 it was concluded that reactions involving aromatics dominate over H-SSZ-24, whereas reactions involving aliphatics were strongly favoured over H-SAPO-5 (Figures 1 and 2). Furthermore, the methylation experiments of benzene and propene displayed in Figure 3 show that while the rate of benzene methylation was significantly higher than that of propene methylation over H-SSZ-24, the two rates were similar over H-SAPO-5. This correlates well with the data presented in Figure 6, which shows that methanol and benzene were more likely to form a pre-reactive complex during MD simulations in H-SSZ-24 than in H-SAPO-5, whereas the reverse was true for methanol and propene.

To assess the sensitivity of the reported probabilities in Figure 6 to the applied cut-off values, the entire analysis was repeated with other cut-off values. While the absolute numbers of the probabilities are prone to change, the relative positions of the four points indicated in Figure 6 are not (see Supporting Information S10).

Methylation reactions can also occur in a stepwise fashion via a framework bound methoxy group [80]. A number of theoretical studies already addressed the importance of a stepwise mechanism. [73, 81-83]. In particular, it has been reported the stepwise mechanism

becomes important at high temperature due to the entropic effect of the intermediate release of a water molecule [73, 82]. A study on the competition between associative and dissociative methanol dehydration was recently presented by Jones and Iglesia. The authors state that methoxy-mediated routes become prevalent at higher temperatures and lower pressures due to an enthalpy-entropy trade-off [84]. The probability for pre-reactive complex formation only applies to the concerted methylation mechanism. However, methanol protonation is a necessary step in both the stepwise and concerted pathways. Indeed, in both mechanisms methanol needs to be protonated to transfer its methyl group either directly to a hydrocarbon molecule or to the framework. We additionally performed MD simulations of both AFI materials loaded with a methoxy group and a co-adsorbed benzene or propene molecule at 350 ºC. Analysis of the shortest distance between the methoxy group and the benzene or propene molecule indicated the same trend as observed for methanol as direct methylating agent. In H-SSZ-24, a significantly shorter average interaction distance was observed for the methoxy – benzene complex (5.71 Å) compared to the methoxy – propene complex (6.04 Å) (Supporting Information, Section S11). In H-SAPO-5, the carbon-carbon interaction distance in the methoxy – propene complex (6.27 Å) was only slightly larger than in the methoxy – benzene complex (6.14 Å). These results indicate that also in case of a stepwise methylation, the adsorption behaviour was significantly different for alkenes and aromatics. For a more detailed analysis as performed in Figure 6, a new index would have to be defined to take into account the orientation of the hydrocarbon with respect to the methoxide.

3.3.2. Reactivity from metadynamics simulations

To further confirm the relationship between the two indices defined in Figure 6 and the reactivity towards methylation, two relatively short metadynamics simulations of benzene and propene methylation in H-SSZ-24 at 350 °C were performed. Three collective variables (coordination numbers) were defined (Figure S12.1) to explicitly sample the direct methylation and the stepwise mechanism via a surface methoxide. Inspection of the metadynamics data revealed that prior to every transition corresponding to a concerted methylation, methanol was protonated and oriented with the methyl carbon towards the co-adsorbed hydrocarbon (Figures S12.2 and S12.3). Prior to transitions corresponding to methoxide group formation, methanol was protonated but no pre-reactive complex for methylation was formed. This means that next to methanol protonation and the fact that enough energy must be available to break a bond, the orientation of methanol with respect to the co-adsorbed hydrocarbon is a crucial factor in the competition between a concerted methylation step and methoxide formation. These observations support the assumption that the two indices that were introduced (methanol protonation and pre-reactive complex formation) are related to reactivity.

Further inspection of the simulations revealed that the direct methylations were the first sampled transitions. As the metadynamics technique in principle first samples the lowest activated transition, the concerted methylation steps were probably lower activated than stepwise methylations under the applied conditions. To obtain accurate free energy surfaces

and thus more detailed insights into activation barriers, longer simulation times are needed, which is beyond the scope of this article.

Figure 7 displays snapshots along the paths sampled during the metadynamics simulations. In particular, transition states and corresponding pre-reactive complexes for concerted benzene or propene methylation reactions are shown. The pre-reactive complexes were formed ca. 100 fs prior to the actual barrier crossings during the simulation and exhibited protonated methanol and a favourable orientation of methanol towards the hydrocarbon. For each case, two geometrically non-equivalent transition states are shown. This suggests that once methanol was protonated and a favourable orientation for methylation was achieved, the reactants could still adopt many configurations inside the channel prior to reaction. In the pre-reactive complex formed prior to methoxide formation, we observed methanol protonation but not favourable orientation of methanol with respect to the hydrocarbon (Figure S12.4). Furthermore, we observed that the transition regions and regions corresponding with the stable states for benzene and propene methylation are all relatively broad in the collective variable space (Figures S12.4 and S12.5). This also emphasized the need for a dynamical-based description of the investigated reactions in the large pore AFI catalysts as the corresponding free energy surface was relatively flat due to a large number of reaction paths corresponding with the same reaction step.

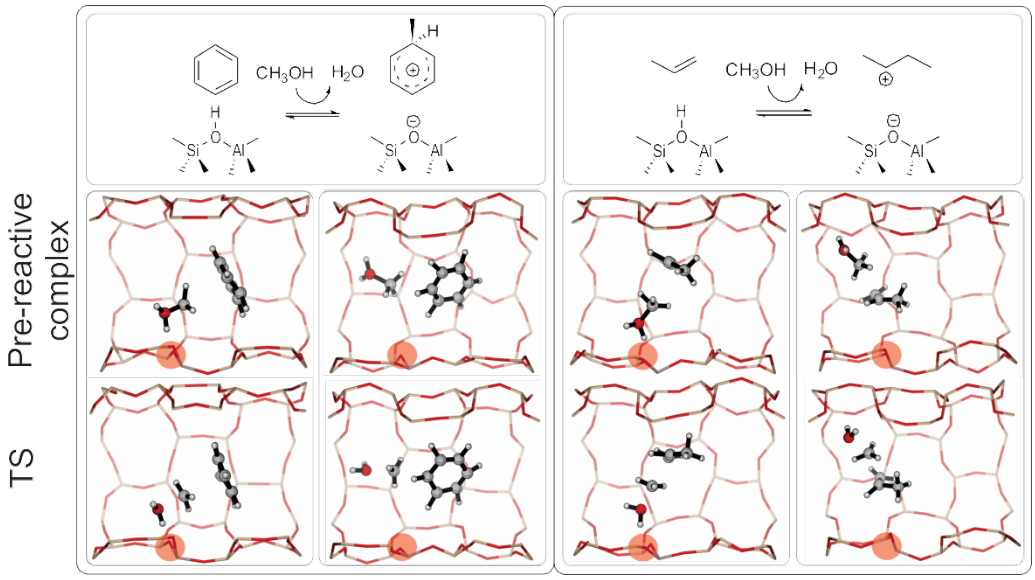

Figure 7: Snapshots of transition states and corresponding pre-reactive complexes (formed 100 fs prior to the barrier crossing) sampled during a 47 ps metadynamics simulation of benzene (left) and propene (right) methylation in H-SSZ-24 at 350 °C. The red circle indicates the original position of the acid site.

Summarized, careful geometrical analysis of the MD trajectories at 350 ºC revealed that the probability to form a pre-reactive complex, combined with the degree of methanol protonation correlates with the reactivity of co-adsorbed methanol and benzene or propene towards methylation reactions. Furthermore, the calculated and experimentally observed reactivity towards methylation of benzene and propene correlates well with the previously observed dominance of product formation from the arene cycle over H-SSZ-24 and the alkene cycle over H-SAPO-5 during the MTH reaction [32].

4. Conclusions

In this study, a thorough assessment of the influence of zeolitic acid strength on zeolite-catalysed reactions was made by co-reaction experiments and molecular simulations of methanol and benzene and methanol and propene in the isostructural AFI materials H-SSZ-24 and H-SAPO-5. In line with what was earlier found for the MTH reaction in both catalysts, H-SAPO-5 clearly favours reactions involving alkenes, even at high benzene partial pressures and lower than 0.3 % benzene conversion at 250°C. A direct comparison of benzene and propene methylation at 350-400 °C further revealed that benzene methylation was significantly faster than propene methylation in H-SSZ-24, whereas the two reactions occur at similar rates in H-SAPO-5. A molecular level understanding of this observation was provided by performing DFT molecular dynamics and metadynamics simulations. As many energy minima may occur at real operating conditions, a molecular dynamics approach was necessary. The probabilities to form favourable methanol – hydrocarbon complexes in the two catalysts, combined with the degree of methanol protonation at 350 ºC could be correlated with the experimentally observed reactivities. In particular, a highly favourable adsorption complex for methanol/benzene co-adsorption combined with a low free energy for methanol protonation in the strongly acidic H-SSZ-24 correlates well with the observed higher reactivity for benzene methylation than propene methylation in this structure. Metadynamics simulations suggested that the concerted methylation step exhibits the lowest activation barrier for benzene and propene methylation under the applied conditions. Moreover, prior to every concerted methylation step, methanol was protonated and a favourable orientation of methanol towards the hydrocarbon was adopted. These theoretical findings provide insight into why the MTO product formation is governed by different catalytic cycles in the two AFI catalysts.

Acknowledgements

This publication is part of the inGAP Centre of Research-based Innovation, which receives financial support from the Norwegian Research Council under Contract No. 174893. In the inGAP centre, zeolite studies are performed in close collaboration with Haldor Topsøe AS. K.D.W. is a PhD fellow funded by the Foundation of Scientific Research - Flanders (FWO). We are grateful to the Research Board of Ghent University and BELSPO in the frame of IAP P7/05. Funding was also received from the European Research Council under the European Community's Seventh Framework Program [FP7(2007-2013) ERC grant agreement number 240483]. Computational resources and services used in this work were provided by the Stevin Supercomputer Infrastructure of Ghent University and by the VSC (Flemish Supercomputer Center), funded by the Hercules Foundation and the Flemish Government – department EWI.

5. References

[1] T. Maesen, in: J. Čejka, H. van Bekkum, A. Corma, F. Schüth (Eds.) Introduction to zeolite science and practice, Elsevier, Amsterdam, 2007, pp. 1.
[2] J.F. Haw, Phys. Chem. Chem. Phys., 4 (2002) 5431.
[3] A.J. Jones, R.T. Carr, S.I. Zones, E. Iglesia, J. Catal., 312 (2014) 58.
[4] C.-M. Wang, R.Y. Brogaard, B.M. Weckhuysen, J.K. Nørskov, F. Studt, J. Phys. Chem. Lett., 5 (2014) 1516.
[5] P. Deshlahra, R.T. Carr, E. Iglesia, J. Am. Chem. Soc., 136 (2014) 15229.
[6] R.J. Gorte, Catal. Lett., 62 (1999) 1.
[7] R.T. Carr, M. Neurock, E. Iglesia, J. Catal., 278 (2011) 78.
[8] A. Zecchina, G. Spoto, S. Bordiga, Phys. Chem. Chem. Phys., 7 (2005) 1627.
[9] A.I. Biaglow, R.J. Gorte, G.T. Kokotailo, D. White, J. Catal., 148 (1994) 779.
[10] D.A. Simonetti, R.T. Carr, E. Iglesia, J. Catal., 285 (2012) 19.
[11] J. Macht, R.T. Carr, E. Iglesia, J. Am. Chem. Soc., 131 (2009) 6554.
[12] V. Van Speybroeck, K. Hemelsoet, K. De Wispelaere, Q. Qian, J. Van der Mynsbrugge, B. De Sterck, B.M. Weckhuysen, M. Waroquier, ChemCatChem, 5 (2013) 173.
[13] U. Olsbye, S. Svelle, M. Bjørgen, P. Beato, T.V.W. Janssens, F. Joensen, S. Bordiga, K.P. Lillerud, Angew. Chem. Int. Ed., 51 (2012) 5810.
[14] K. Hemelsoet, J. Van der Mynsbrugge, K. De Wispelaere, M. Waroquier, V. Van Speybroeck, ChemPhysChem, 14 (2013) 1526.
[15] M. Stöcker, Microporous Mesoporous Mater., 29 (1999) 3.
[16] S. Ilias, A. Bhan, ACS Catal., 3 (2013) 18.
[17] J.F. Haw, W.G. Song, D.M. Marcus, J.B. Nicholas, Acc. Chem. Res., 36 (2003) 317.
[18] I.M. Dahl, S. Kolboe, J. Catal., 161 (1996) 304.
[19] I.M. Dahl, S. Kolboe, J. Catal., 149 (1994) 458.
[20] I.M. Dahl, S. Kolboe, Catal. Lett., 20 (1993) 329.
[21] M. Bjørgen, S. Svelle, F. Joensen, J. Nerlov, S. Kolboe, F. Bonino, L. Palumbo, S. Bordiga, U. Olsbye, J. Catal., 249 (2007) 195.
[22] S. Svelle, F. Joensen, J. Nerlov, U. Olsbye, K.-P. Lillerud, S. Kolboe, M. Bjørgen, J. Am. Chem. Soc., 128 (2006) 14770.
[23] S. Teketel, U. Olsbye, K.P. Lillerud, P. Beato, S. Svelle, Microporous Mesoporous Mater., 136 (2010) 33.
[24] S. Teketel, S. Svelle, K.P. Lillerud, U. Olsbye, ChemCatChem, 1 (2009) 78.
[25] M. Bjørgen, S. Akyalcin, U. Olsbye, S. Benard, S. Kolboe, S. Svelle, J. Catal., 275 (2010) 170.
[26] S. Svelle, U. Olsbye, F. Joensen, M. Bjørgen, J. Phys. Chem. C, 111 (2007) 17981.
[27] M. Bjørgen, F. Joensen, K.-P. Lillerud, U. Olsbye, S. Svelle, Catal. Today, 142 (2009) 90.
[28] M. Bjørgen, U. Olsbye, D. Petersen, S. Kolboe, J. Catal., 221 (2004) 1.
[29] J.H. Ahn, B. Temel, E. Iglesia, Angew. Chem. Int. Ed., 48 (2009) 3814.
[30] D.A. Simonetti, J.H. Ahn, E. Iglesia, J. Catal., 277 (2011) 173.
[31] M. Westgård Erichsen, S. Svelle, U. Olsbye, J. Catal., 298 (2013) 94.
[32] M. Westgård Erichsen, S. Svelle, U. Olsbye, Catal. Today, 215 (2013) 216.
[33] J. Sauer, K.P. Schroder, V. Termath, Collect. Czech. Chem. Commun., 63 (1998) 1394.
[34] S. Bordiga, L. Regli, D. Cocina, C. Lamberti, M. Bjørgen, K.P. Lillerud, J. Phys. Chem. B, 109 (2005) 2779.
[35] R. Shah, J. D. Gale, M. C. Payne, Chem. Commun., (1997) 131.

[36] S. Teketel, M. Westgård Erichsen, F. Lønstad Bleken, S. Svelle, K.P. Lillerud, U. Olsbye, in: Catalysis: Volume 26, The Royal Society of Chemistry, 2014, pp. 179.
[37] J.E. Bercaw, P.L. Diaconescu, R.H. Grubbs, R.D. Kay, S. Kitching, J.A. Labinger, X.W. Li, P. Mehrkhodavandi, G.E. Morris, G.J. Sunley, P. Vagner, J. Org. Chem., 71 (2006) 8907.
[38] S.L.C. Moors, K. De Wispelaere, J. Van der Mynsbrugge, M. Waroquier, V. Van Speybroeck, ACS Catal., 3 (2013) 2556.
[39] O. Kresnawahjuesa, R.J. Gorte, D. de Oliveira, L.Y. Lau, Catal. Lett., 82 (2002) 155.
[40] R.J. Gorte, Catal. Today, 28 (1996) 405.
[41] J. VandeVondele, M. Krack, F. Mohamed, M. Parrinello, T. Chassaing, J. Hutter, Comput. Phys. Commun., 167 (2005) 103.
[42] J. Hutter, M. Iannuzzi, F. Schiffmann, J. VandeVondele, Wiley Interdiscip. Rev.: Comput. Mol. Sci., 4 (2014) 15.
[43] G. Lippert, J. Hutter, M. Parrinello, Theor. Chem. Acc., 103 (1999) 124.
[44] G. Lippert, J. Hutter, M. Parrinello, Mol. Phys., 92 (1997) 477.
[45] K. Yang, J.J. Zheng, Y. Zhao, D.G. Truhlar, J. Chem. Phys., 132 (2010) 10.
[46] S. Goedecker, M. Teter, J. Hutter, Phys. Rev. B, 54 (1996) 1703.
[47] S. Grimme, J. Antony, S. Ehrlich, H. Krieg, J. Chem. Phys., 132 (2010) 19.
[48] A.N. Mlinar, P.M. Zimmerman, F.E. Celik, M. Head-Gordon, A.T. Bell, J. Catal., 288 (2012) 65.
[49] D. Frenkel, B. Smit, Understanding molecular simulations, second edition ed., Academic press, Elsevier, 2002.
[50] S. Svelle, C. Tuma, X. Rozanska, T. Kerber, J. Sauer, J. Am. Chem. Soc., 131 (2009) 816.
[51] V. Van Speybroeck, J. Van der Mynsbrugge, M. Vandichel, K. Hemelsoet, D. Lesthaeghe, A. Ghysels, G.B. Marin, M. Waroquier, J. Am. Chem. Soc., 133 (2010) 888.
[52] J. Van der Mynsbrugge, M. Visur, U. Olsbye, P. Beato, M. Bjørgen, V. Van Speybroeck, S. Svelle, J. Catal., 292 (2012) 201.
[53] J. Van der Mynsbrugge, J. De Ridder, K. Hemelsoet, M. Waroquier, V. Van Speybroeck, Chem. Eur. J., 19 (2013) 11568.
[54] A. Laio, M. Parrinello, Proc. Natl. Acad. Sci. U. S. A., 99 (2002) 12562.
[55] A. Laio, F.L. Gervasio, Rep. Prog. Phys., 71 (2008).
[56] L. Benco, T. Bucko, J. Hafner, J. Catal., 277 (2011) 104.
[57] T. Bucko, L. Benco, O. Dubay, C. Dellago, J. Hafner, J. Chem. Phys., 131 (2009).
[58] T. Bucko, L. Benco, J. Hafner, J.G. Angyan, J. Catal., 279 (2011) 220.
[59] F. Goltl, J. Hafner, Microporous Mesoporous Mater., 166 (2013) 176.
[60] P.M. Zimmerman, D.C. Tranca, J. Gomes, D.S. Lambrecht, M. Head-Gordon, A.T. Bell, J. Am. Chem. Soc., 134 (2012) 19468.
[61] J. Gomes, M. Head-Gordon, A.T. Bell, J. Phys. Chem. C, 118 (2014) 21409.
[62] V. Van Speybroeck, K. De Wispelaere, J. Van der Mynsbrugge, M. Vandichel, K. Hemelsoet, M. Waroquier, Chem. Soc. Rev., 43 (2014) 7326.
[63] I. Hill, A. Malek, A. Bhan, ACS Catal., 3 (2013) 1992.
[64] B. Arstad, S. Kolboe, O. Swang, J. Phys. Chem. B, 106 (2002) 12722.
[65] J.H. Ahn, R. Kolvenbach, S.S. Al-Khattaf, A. Jentys, J.A. Lercher, ACS Catal., 3 (2013) 817.
[66] D. Lesthaeghe, B. De Sterck, V. Van Speybroeck, G.B. Marin, M. Waroquier, Angew. Chem. Int. Ed., 46 (2007) 1311.
[67] W. Dai, W. Kong, G. Wu, N. Li, L. Li, N. Guan, Catal. Commun., 12 (2011) 535.

[68] G. Lischke, B. Parlitz, U. Lohse, E. Schreier, R. Fricke, Appl. Catal. A, 166 (1998) 351.
[69] J. Chen, P.A. Wright, S. Natarajan, J.M. Thomas, Stud. Surf. Sci. Catal., 84 (1994) 1731.
[70] B. Zibrowius, E. Loffler, M. Hunger, Zeolites, 12 (1992) 167.
[71] S.G. Hedge, P. Ratnasamy, L.M. Kustov, V.B. Kazansky, Zeolites, 8 (1988) 137.
[72] S. Svelle, S. Kolboe, O. Swang, U. Olsbye, J. Phys. Chem. B, 109 (2005) 12874.
[73] R.Y. Brogaard, R. Henry, Y. Schuurman, A.J. Medford, P.G. Moses, P. Beato, S. Svelle, J.K. Nørskov, U. Olsbye, J. Catal., 314 (2014) 159.
[74] J. Van der Mynsbrugge, S.L.C. Moors, K. De Wispelaere, V. Van Speybroeck, ChemCatChem, 6 (2014) 1906.
[75] S. Svelle, P.O. Rønning, U. Olsbye, S. Kolboe, J. Catal., 234 (2005) 385.
[76] F. Haase, J. Sauer, Microporous Mesoporous Mater., 35-6 (2000) 379.
[77] J.D. Gale, R. Shah, M.C. Payne, I. Stich, K. Terakura, Catal. Today, 50 (1999) 525.
[78] S. Bordiga, L. Regli, C. Lamberti, A. Zecchina, M. Bjørgen, K.P. Lillerud, J. Phys. Chem. B, 109 (2005) 7724.
[79] G. Sastre, D.W. Lewis, A. Corma, Phys. Chem. Chem. Phys., 2 (2000) 177.
[80] S. Svelle, M. Visur, U. Olsbye, S. Saepurahman, M. Bjørgen, Top. Catal., 54 (2011) 897.
[81] M.N. Mazar, S. Al-Hashimi, A. Bhan, M. Cococcioni, J. Phys. Chem. C, 116 (2012) 19385.
[82] A.M. Vos, K.H.L. Nulens, F. De Proft, R.A. Schoonheydt, P. Geerlings, J. Phys. Chem. B, 106 (2002) 2026.
[83] T. Maihom, B. Boekfa, J. Sirijaraensre, T. Nanok, M. Probst, J. Limtrakul, J. Phys. Chem. C, 113 (2009) 6654.
[84] A.J. Jones, E. Iglesia, Angew. Chem. Int. Ed., 53 (2014) 12177.
[85] S. Svelle, P.O. Rønning, S. Kolboe, J. Catal., 224 (2004) 115.
[86] I.M. Hill, S.A. Hashimi, A. Bhan, J. Catal., 291 (2012) 155.